PHYSICAL REVIEW B

CONDENSED MATTER

THIRD SERIES, VOLUME 28, NUMBER 5 1 SEPTEMBER 1983

Magnetic properties of actinide elements having the $5f^6$ and $5f^7$ electronic configurations

S. E. Nave
Physics Department, University of Tennessee, Knoxville, Tennessee 37996

R. G. Haire
Transuranium Research Laboratory, Chemistry Division, Oak Ridge National Laboratory, Oak Ridge, Tennessee 37830

Paul G. Huray
Physics Department, University of Tennessee, Knoxville, Tennessee 37996
and Transuranium Research Laboratory, Chemistry Division, Oak Ridge National Laboratory, Oak Ridge, Tennessee 37830

(Received 16 July 1982; revised manuscript received 11 May 1983)

Magnetic susceptibility measurements have been made on multimicrogram quantities of $^{243}AmF_3$, $^{248}CmF_4$, $^{248}CmO_2$, and $^{248}CmBaO_3$ samples (nominally the $5f^6$ electronic configuration) and on $^{248}Cm_2O_3$, $^{248}CmF_3$, $^{249}BkF_4$, and $^{249}BkO_2$ (nominally the $5f^7$ electronic configuration) in the temperature range 4.2–300 K and in magnetic fields up to 1650 G. The experimentally determined effective magnetic moments and the Curie-Weiss constants for these compounds are presented. The deviation of the moments for the $5f^6$ compounds from those expected from classic theory is discussed in terms of low-lying excited states, chemical composition, crystal-field perturbations, and realistic electronic structure.

I. INTRODUCTION

In principle, the actinide series ($5f$) and the lanthanide series ($4f$) of elements are characterized by the progressive filling of f orbitals with increasing atomic number. However, in the actinide metals this process is actually realized only after plutonium, due to the closeness in energy of the $5f$ and $6d$ orbitals and the resulting hybridization in the earlier actinide elements. The major differences between the transplutonium elements and their lanthanide counterparts are the larger spatial extension and the larger spin-orbit coupling energy of the $5f$ wave functions. The $4f$ configurations have localized moments, and experimental values for the paramagnetic effective moments are in good agreement with calculated values, assuming the ground state is defined by Hund's-rule and L-S coupling. Thus it is of great interest to see if ionic compounds of the actinide series follow the same magnetic systematics as found for the lanthanide series.

The paramagnetic effective moments are determined by measuring the susceptibility as a function of temperature. For a system of slightly interacting local moments the susceptibility χ is given by[1]

$$\chi = N\mu_{\text{eff}}^2/3k(T+\Theta_p) . \quad (1)$$

Here N is the number of ions per unit volume, k is Boltzmann's constant, and T is the absolute temperature. If Hund's-rule and L-S coupling are valid, then the theoretical $\mu_{\text{eff}}=g[J(J+1)]^{1/2}$ (where the Landé

$$g=1+[J(J+1)+S(S+1)-L(L+1)]/2[J(J+1)] , \quad (2)$$

and J is the total angular-momentum quantum number for the Hund's-rule ground state). The term Θ_p is the paramagnetic Weiss temperature. It is a measure of the interaction between the spins of neighboring atoms and describes the average magnetic environment in which each heavy atom finds itself.

Figure 1 shows the experimentally determined[2] effective magnetic moments for a series of lanthanide compounds. The solid line in the figure connects the theoretical magnetic moments derived by assuming that the ground state is defined by Hund's-rule and L-S coupling, and that an excited state is not close enough to the ground state to be thermally populated to a significant degree over the experimental temperature range. From this figure we see substantial departure between simple theory and experiment only near the $4f^6$ configuration. Van Vleck[3] explained this difference for Eu by invoking the presence of a $J=1$ excited state near the $J=0$ ground state, and was able to

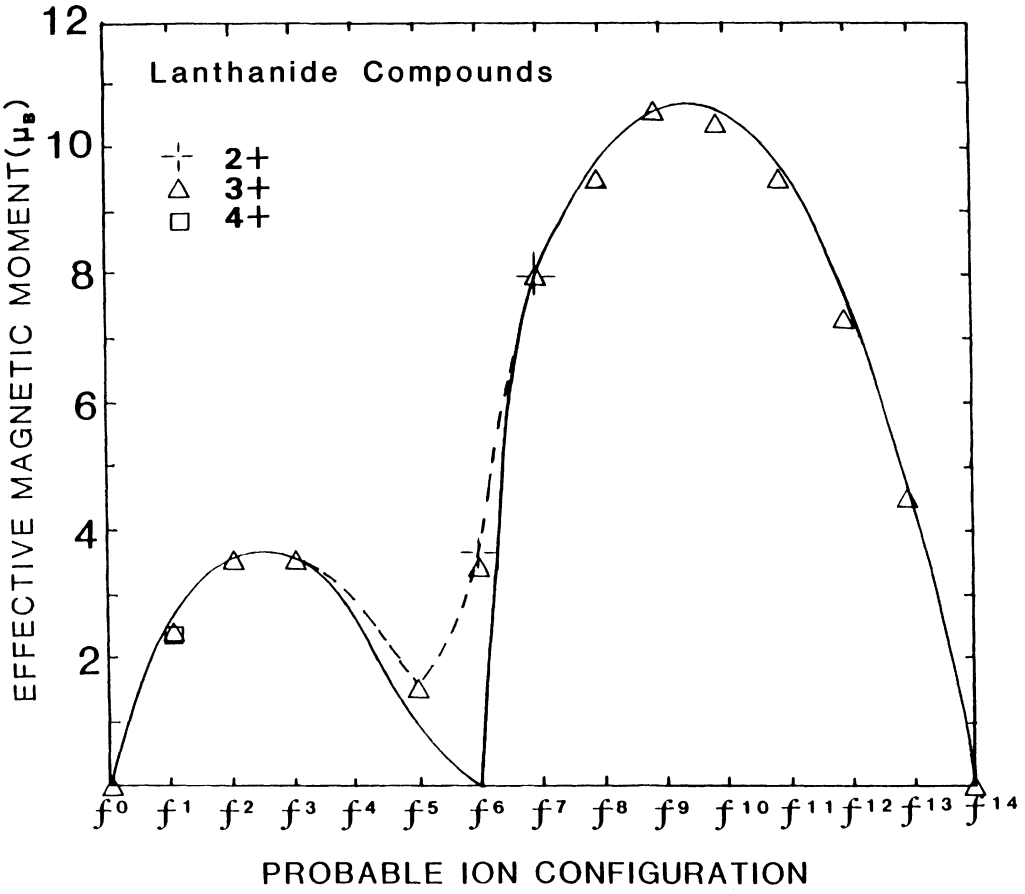

Fig. 1. Experimental effective magnetic moments of lanthanide compounds as a function of their probable electronic configuration near 300 K. The solid line connects the theoretical values of expected magnetic moments of the respective ionic configuration using simple L-S coupling and Hund's rule for the ground states. The dotted line connects the theoretical values of the same states but additionally assumes a thermal population of excited states at 300 K according to a Van Vleck multiplet correction.

produce a room-temperature theoretical estimation of the effective magnetic moments, as shown by the dotted-line connector. The dotted values have since been verified through optical-absorption experiments by Hessler and Carnall[4] which suggest low-lying excited states above the ground states at $\Delta=0.9$, 0.12, 0.04, and 3.95 eV in the cases of $_{61}Pm^{3+}$, $_{62}Sm^{3+}$, $_{63}Eu^{3+}$, and $_{64}Gd^{3+}$, respectively. The first three excited states are low enough in energy to be at least partially populated at 300 K, where $kT=0.026$ eV (e.g., for Eu^{3+}, $e^{-\Delta/kT}=0.24$).

Compounds of the actinides with the larger spatial extent of the $5f$ electrons would be expected to follow the same magnetic systematics as the lanthanide compounds only if (1) the degree of localization and lattice spacing are such that interactions with near neighbors are small and (2) if the ground state is close to that described by L-S coupling and Hund's rule. If they are like their lanthanide homologs, AmF_3, CmF_4, CmO_2, and $BaCmO_3$ should be ioniclike compounds corresponding to the $5f^6$ electronic configuration, and Cm_2O_3, CmF_3, BkF_4, and BkO_2 should be ioniclike compounds corresponding to the $5f^7$ configuration. Hund's-rule and L-S coupling lead to the theoretical value of $0\mu_B$ for the paramagnetic effective moment of the f^6 ($J=0$) configuration, whereas the f^7 configuration, with $J=\frac{7}{2}$, has an expected effective moment of $7.94\mu_B$.

However, L-S coupling may not be the most appropriate scheme for describing the ground-state wave function. Indeed, an intermediate coupling model between L-S and j-j coupling[5] may be necessary to describe the wave function, due to the large spin-orbit coupling. In this model the spin-orbit term in the Hamiltonian is taken into account as a perturbation with the $|L,S,J\rangle$ states as a basis set. This perturbation admixes the states of the same J value but different L and S values into the ground state. For the $5f^6$ and $5f^7$ configurations the Hund's-rule L-S states make up only 47% (Ref. 5) and 79% (Ref. 6), respectively, of the intermediate wave functions. The calculated effective moment for the $5f^7$ state in this intermediate coupling model is $7.55\mu_B$ and is only slightly different from the $7.94\mu_B$ value above. For the $5f^6$ configuration, identical values are obtained from both approaches since $\mu_{\text{eff}}=g[J(J+1)]^{1/2}$ and J is zero for all of the admixed states.

II. EXPERIMENTAL

A. Sample material

The transplutonium elements used in this study were made available through the U.S. Department of Energy,

Division of Chemical Sciences program of transplutonium element production and research. Purification of the materials was performed by ion exchange and chromatographic techniques previously reported.[7,8] The isotopic composition for each element was as follows: (1) Am, 100% of isotope 243, (2) Cm, 97% of isotope 248 with the remainder mainly 246, and (3) Bk, 100% of isotope 249.

The trifluorides were prepared by precipitation by adding electrolytic grade HF to a 0.1*M* HCl solution of the trivalent actinide. The washed precipitates were dried under flowing argon at 200 °C to yield the trifluoride. No effort was made to prepare a totally anhydrous trifluoride. The trifluorides are not hygroscopic like the heavier trihalides and satisfactory trifluorides can be prepared by this technique.

The tetrafluorides required more extensive treatment and were prepared from the trifluoride materials by (1) treatment with a flowing-fluorine atmosphere at 550 °C, (2) a three-day to two-week fluorination period at 400 °C under 3—4 atm of fluorine, and (3) cooling under 3—4 atm of fluorine using a programmed cooling sequence. During the second and third steps, the fluorine atmosphere was changed several times to assure the desired atmosphere. The cooling sequence consisted of steps of ≤ 50 °C with hold periods of 2 h to a day after each step. After fluorination the tetrafluorides were maintained in helium atmospheres, often individual samples were immediately sealed in a quartz capillary under a $\sim \frac{3}{4}$ atm of helium.

Both berkelium and curium oxides were prepared by precipitating the trivalent actinides with oxalate ion from a 0.1*M* HCl solution, and then calcining the oxalates in oxygen up to 1000 °C to assure the removal of carbon and/or carbonate residues. This procedure provided BkO_2 directly. Such a procedure produced curium oxides of unknown oxygen to curium ratios ($1.5 < [O]/[Cm] < 2.0$), the composition of curium oxide obtained being a function of oxygen overpressure, temperature, and time.[9] Sesquioxide samples were obtained from the oxalate product by heating to 1100 °C in carbon monoxide and/or in high vacuum ($< 10^{-6}$ mm Hg), and then rapidly cooling under the same conditions. This high-temperature procedure produced the monoclinic crystal form of Cm_2O_3. The curium dioxide samples were obtained from the calcined oxalate product by heating at lower temperature in 4—5 atm of research-grade oxygen. The oxidation procedure consisted of heating to 500 °C for half a day, sequentially cooling to 375 °C in increments of 25 °C with hold periods of 2 h at each step. The sample was held at 375 °C for one day, cooled to 350°, and held for up to three weeks at this temperature. The final cooldown to room temperature took place in increments of 50 °C.

Curium oxides were also prepared by thermally decomposing a hydrated curium nitrate salt at 700 °C in air, yielding an oxide product with an [O]/[Cm] ratio of 1.95 (as determined by x ray). The lower calcination temperature avoided the formation of monoclinic Cm_2O_3, which is more difficult to reoxidize than the cubic-related forms of curium oxides.[9] Monoclinic sesquioxide samples were obtained from the calcined nitrate product by reduction in carbon monoxide or vacuum at 1100 °C, while the body-centered sesquioxide samples were obtained by reduction under the same conditions at 800 °C. The dioxide samples were obtained from the calcined nitrate product by using the same oxidation procedure employed for the oxalate derived material.

The $BaCmO_3$ compound, in which Cm(IV) should be stabilized, was prepared by mixing nitrate solutions of barium and trivalent curium (1.1Ba:1.0Cm to assure sufficient Ba), evaporating the resulting solution to dryness, and then calcining the solids to 700 °C in oxygen. These products were then subjected to further treatment. Some were cooled slowly to 350 °C in 1 atm of oxygen, where they were maintained for $\sim \frac{1}{2}$ day before cooling to room temperature. Other samples were heated to and held for 1—2 days at 1000 °C in oxygen to improve their crystallinity. These latter samples were then cooled using two different procedures: (1) They were cooled and held at 350 °C as described above and (2) they were cooled under 4 atm of oxygen to 350 °C, being held at this temperature for three days before cooling to room temperature. These procedures were used to provide the best conditions for attaining the tetravalent state of curium.

B. Sample analysis

X-ray analyses of the samples used both Cu $K\alpha$ and Mo $K\alpha$ radiation in conjunction with 57- and 114-mm Debye-Scherrer powder cameras. Lattice parameters were calculated with the computer program LCR-2,[10] including the Nelson-Riley extrapolation function. Mass spectroscopic analyses of the samples were performed using a standard spark-source mass spectroscopy technique.[11]

Optical-absorption measurements on some of the solid samples were obtained with a single-beam microscope spectrophotometer.[12] The range of these measurements were limited to a region from 9×10^3 cm^{-1} ($\sim$1 eV) to 34×10^3 cm^{-1} ($\sim$4 eV).

C. Magnetic data collection and analysis

Measurements of magnetism of the metals and compounds of transplutonium actinides generally involve small sample quantities due to self-heating of these radioactive elements and their limited availability. We have, therefore, constructed a SQUID-based (superconducting quantum interference device) micromagnetic susceptometer for use with samples as small as 1 μg; it is this instrument which has been used for the current set of measurements. The apparatus and technique of measurements has been previously described,[13] although minor modifications have been made to the original sample holder (see Fig. 2).

Experience has shown that sample temperature can be adequately determined by means of a copper-constantan thermocouple attached to the gold wire holding the sample. A uniform thermal environment for the sample is achieved by adding a small sapphire tube around the gold wire, which is, in turn, located inside a quartz insulating tube.

In cases where chemical stability of the sample might be

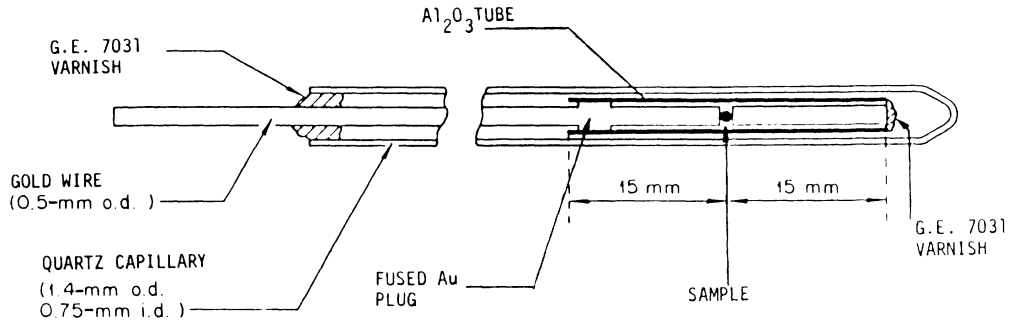

FIG. 2. A typical sample-holder cross section used for the thermal isolation of samples in this study. The actinide compounds were sometimes additionally encapsulated in small helium-filled quartz capillaries to ensure chemical stability.

influenced by exposure to nitrogen, oxygen, or water vapor, we have encapsulated the samples in small quartz capillaries filled with helium before insertion into the sapphire tubes. Although there is a potential danger of a temperature differential between the thermocouple and the sample with this arrangement, in practice it has been found to be insignificant as determined by measurements on samples using both types of sample holders. The quartz capillary appears to be the preferred arrangement for this type of sample but for small samples with small paramagnetic moments, the temperature-independent susceptibility of the quartz can add a significant contribution to the magnetic signal.

The paramagnetic effective moments were determined for the samples from a least-squares, straight-line fit to a plot of the inverse susceptibility versus temperature data. The two constants obtained from the fit give μ_{eff} and Θ_p in the theoretical Curie-Weiss formula for the susceptibility χ [Eq. (1)].

In cases where slight curvature is noticeable in the plots of inverse susceptibility versus temperature, a third constant, χ_0, is added as a temperature-independent contribution to the susceptibility. A nonlinear least-squares fit of the data to an expression of the form

$$\chi=\chi_0+N\mu_{\text{eff}}^2/3k(T+\Theta_p) \tag{3}$$

is performed for these cases. In this approach there are three fitting parameters, μ_{eff}, Θ_p, and χ_0 that need to be determined.

In cases for which the samples were encapsulated in quartz holders, the mathematically determined parameter, χ_0, is strongly influenced by the sample-holder susceptibility and is neither consistent from sample to sample, nor does it accurately reflect the temperature-independent paramagnetism of the material. In the case of AmF_3, however, we have made special attempts to determine χ_0 by eliminating the quartz holder. This material was thought to be chemically stable enough to allow exposure to nitrogen, oxygen, and water vapor. It is the only reliable χ_0 value which may be identified with the actinide compound alone.

III. RESULTS

A. Magnetic measurements

The paramagnetic effective moments of the BkF_4 and BkO_2 samples were determined from a least-squares, straight-line fit to a plot of the inverse susceptibility versus temperature as shown in Fig. 3. The two constants, μ_{eff} and Θ_p, obtained from the fit are presented in Table I. For the BkO_2 data taken at 1603 G the fit was made only for points in the temperature range 50–200 K. This is due to the sudden unexplained change in slope in these data above 200 K, which was not observed in the data taken at 1200 G. With AmF_3, Cm_2O_3, CmF_3, CmF_4, CmO_2, and $BaCmO_3$, the inverse susceptibility versus temperature

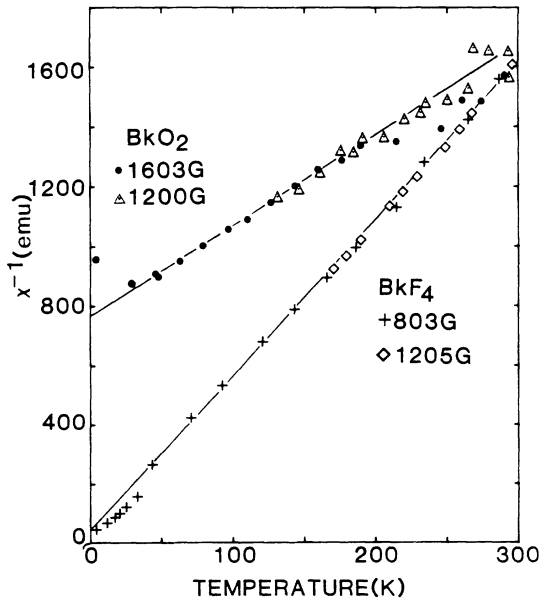

FIG. 3. Inverse magnetic susceptibility of $^{249}BkF_4$ at 803 and 1205 G and $^{249}BkO_2$ at 1200 and 1603 G as a function of temperature. The solid straight lines are a theoretical least-squares fit of the data to a Curie-Weiss variation [Eq. (1)].

TABLE I. Magnetic data and sample masses. Stated errors are those determined from the least-squares-fitting routine.

	Sample	Mass (μg) of actinide	χ_0 (emu/mole)	Θ_p (K)	μ_{eff} (μ_B)
f^6	AmF_3	901.5	$714\times10^{-6}\pm1\%$	1.8	0.63
	CmO_2 no. 1	150.5	$1900\times10^{-6}\pm9\%$	$+12\pm2$	1.63 ± 0.04
	CmO_2 no. 2	122.4	$4100\times10^{-6}\pm4\%$	$+26\pm1$	1.96 ± 0.03
	CmO_2 no. 3	27.6	$2464\times10^{-6}\pm50\%$	$+25\pm14$	2.27 ± 0.20
	$BaCmO_3$ no. 1	197.4	$2130\times10^{-6}\pm10\%$	$+30\pm6$	1.63 ± 0.06
	$BaCmO_3$ no. 2	808.5	$988\times10^{-6}\pm2\%$	18 ± 0.6	1.71 ± 0.01
	CmF_4 no. 1	164.9	$328\times10^{-6}\pm44\%$	-1.2 ± 1.3	3.24 ± 0.04
	CmF_4 no. 2	54.3	$1700\times10^{-6}\pm31\%$	-2.3 ± 4.1	3.49 ± 0.07
	CmF_4 no. 3	100.3	$2800\times10^{-6}\pm8\%$	-4.4 ± 1.5	3.04 ± 0.03
f^7	CmF_3	36.1	$5928\times10^{-6}\pm5\%$	-3.6 ± 0.6	7.67 ± 0.04
	Cm_2O_3 (monoclinic)	27.8		130.0 ± 25	7.74 ± 0.04
	Cm_2O_3 (bcc)	92.1	$3659\times10^{-6}\pm19\%$	110 ± 5	7.51 ± 0.15
	BkF_4	33.9		6.9 ± 1.5	7.93 ± 0.03
	BkO_2	50.2		250.0 ± 50	7.92 ± 0.1

plots showed significant curvatures which required the determination of the third fitting parameter, χ_0 (see experimental section). Plots for the best characterized samples of all but AmF_3 are shown in Figs. 4–7 and the three constants, μ_{eff}, Θ_p, and χ_0, are given in Table I. In the case of AmF_3 the curvature is so large, due to the small μ_{eff} and Θ_p values, that χ_0 can be more accurately determined by a different method. Here it is assumed that Θ_p is zero and a straight line is fitted to a plot of $\chi_m T$ vs T as shown in Fig. 8.

As seen in Table I, the experimentally determined μ_{eff} values for the compounds CmF_3, Cm_2O_3, BkF_4, and BkO_2 are in good agreement with a localized $5f^7$ ionic model where μ_{eff} (theory)$=7.94\mu_B$. The CmF_3 and Cm_2O_3 values are also in good agreement with results of work by others.[14,15] In addition, the small Θ_p values for CmF_3 and BkF_4 support the localized f-electron model, since Θ_p is strongly influenced by the degree of overlap of the $5f$ electronic wave functions. The magnitude of Θ_p should be small (<10 K) for nonoverlapping wave functions as expected for an ionic solid. This is illustrated by data for hydrated sulfates,[3,16] of the lanthanide homologs, Gd and Tb, and other ionic lanthanide compounds[3,16] for which

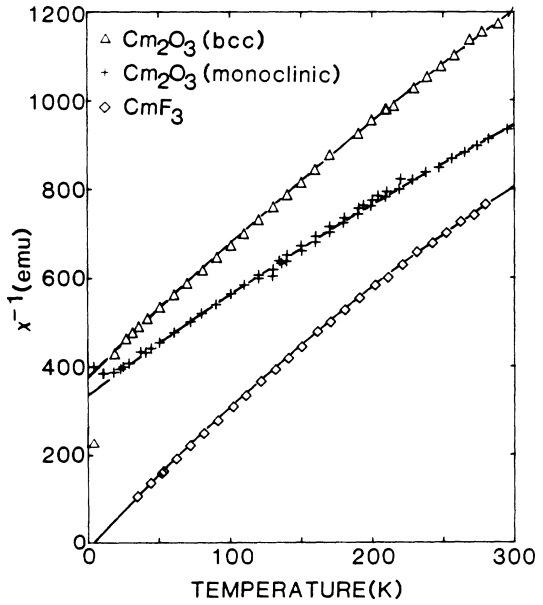

FIG. 4. Inverse magnetic susceptibility as a function of temperature for Cm_2O_3 (bcc), Cm_2O_3 (monoclinic), and CmF_3 samples at ~1600 G. The fit procedure described in the text yields the χ_0, μ_{eff}, and Θ_p given in Table I and produces a nonlinear χ^{-1} vs temperature given by the solid lines and Eq. (3). Here the χ^{-1} vs temperature parameters are determined only for data above 50 K for Cm_2O_3 (monoclinic) since an antiferromagnetic transition at 35 K influences the low-temperature data.

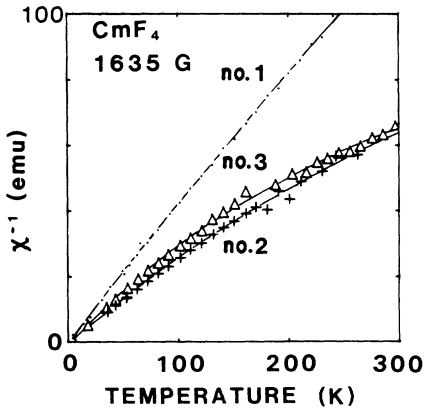

FIG. 5. Inverse magnetic susceptibility as a function of temperature for three different CmF_4 samples of various weights at ~1600 G. As in Fig. 4, the χ^{-1} vs temperature parameters used in Eq. (3) are listed in Table I and produce the nonlinear solid lines shown.

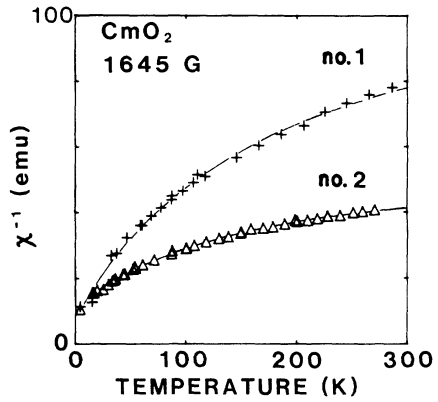

FIG. 6. Inverse magnetic susceptibility as a function of temperature for two different CmO_2 samples at 1645 G. As in Fig. 4, the χ^{-1} vs temperature parameters used in Eq. (3) are listed in Table I and produce the nonlinear solid lines shown.

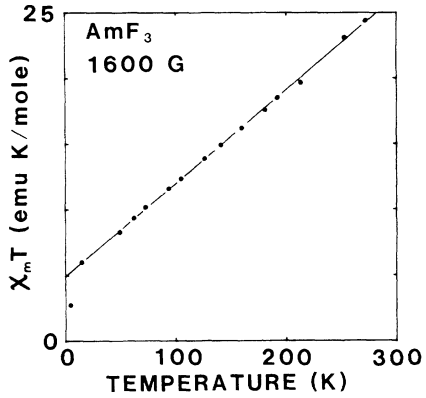

FIG. 8. Magnetic susceptibility times temperature for a 901.5-μg $^{243}AmF_3$ sample at 1600 G as a function of temperature. The solid straight-line fit to the data shows how a sample with a large constant susceptibility, χ_0, and small Θ_p [Eq. (3)] behaves. The slope of this fit was consequently used to remove χ_0 from the experimental data. The resulting inverse residual $(\chi-\chi_0)^{-1}$ follows a linear relation when plotted vs temperature. In this case the fit sequence yields $\chi_0=714\times10^{-6}$ emu/mole, $\mu_{\text{eff}}=0.63\mu_B$, and $\Theta_p=1.8$ K.

Θ_p is near 0 K. In the cases of Cm_2O_3 and BkO_2, their μ_{eff} values also agree with a localized $5f^7$ ionic model, but for these compounds Θ_p is large. These observations, together with the observed magnetic ordering for Cm_2O_3 and BkO_2, are indicative of a strong coupling between reasonably localized moments. Such a large difference between $-\Theta$ and the transition temperatures, T_N, has also been observed for many antiferromagnetic transition-metal compounds.[17] The ratio $-\Theta/T_N$ is only required to be near unity in a simple two-sublattice molecular-field model. If one considers interactions with second, or more distant, near neighbors, large values are theoretically possible for this ratio.[17]

Of these nominally $5f^6$ compounds, only AmF_3 yields the near-zero moment expected for μ_{eff}. A variation in moments was determined for the CmF_4 and CmO_2 samples with the lowest value being obtained for the CmO_2 samples.

The large mass of the AmF_3 sample together with its small μ_{eff} ($0.63\mu_B$) permitted an accurate determination of χ_0 (714×10^{-6} emu/mole). Our data are in substantial agreement with measurements that have been made on another nominally pure Am^{3+} sample,[18] $Am(C_5H_5)_3$, where χ_0 was 715×10^{-6} emu/mole. The small, but nonzero, moment in that compound was attributed[18] to the presence of 0.12 at.% Am^{2+} in their samples ($5f^7$ configuration). The Am^{2+} state is not a common oxidation state for this element and its presence in our AmF_3 samples is not reasonable. Attributing the nonzero moment to the possible presence of Am^{4+} is also not reasonable since it would require large amounts (55%) due to the small theoretical moment of the f^5 configuration ($0.83\mu_B$).

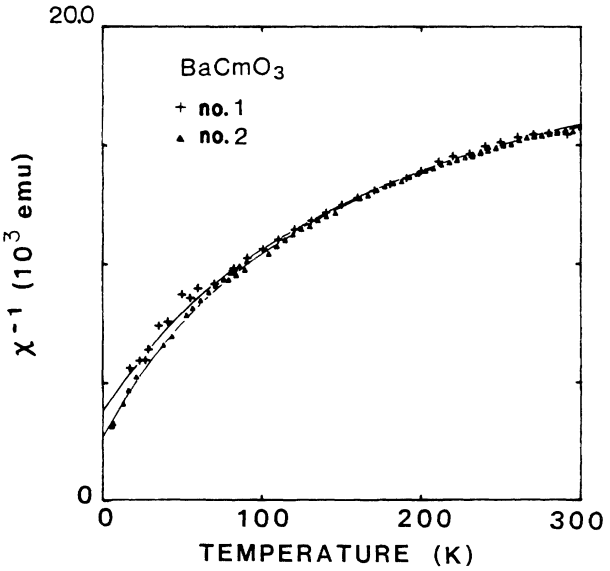

FIG. 7. Inverse magnetic susceptibility as a function of temperature for the two $BaCmO_3$ samples at $\sim$1600 G. As in Fig. 4, the χ^{-1} vs temperature parameters used in Eq. (3) are listed in Table I and produce the nonlinear solid lines shown.

actinide compounds are plotted as a function of expected f-electron configuration, using the values determined in this work and literature values for the lighter actinides[19] and for berkelium[20] (BkF_3 and Bk_2O_3 f^8 configuration). The zero moments expected from simple theory were not experimentally observed for the $5f^6$ Cm(IV) compounds, and the deviations were too great to be explained merely by the experimental limits of the measurements. From the data, it is apparent that both the CmO_2 and the $BaCmO_3$ samples gave the lowest moments.

From the standpoint of electronegativity and oxidation potentials, fluorine would be expected to more readily produce a Cm^{4+} compound than oxygen. However, other factors may be more important. For example, there is a significant crystal modification in going from trigonal CmF_3 to monoclinic CmF_4, as compared to oxidizing the cubic form of Cm_2O_3 to form the face-centered-cubic (fcc) CmO_2. Based on the above and the fact that relatively low preparative temperatures are required to avoid decomposition of the tetravalent compounds, the oxide system may

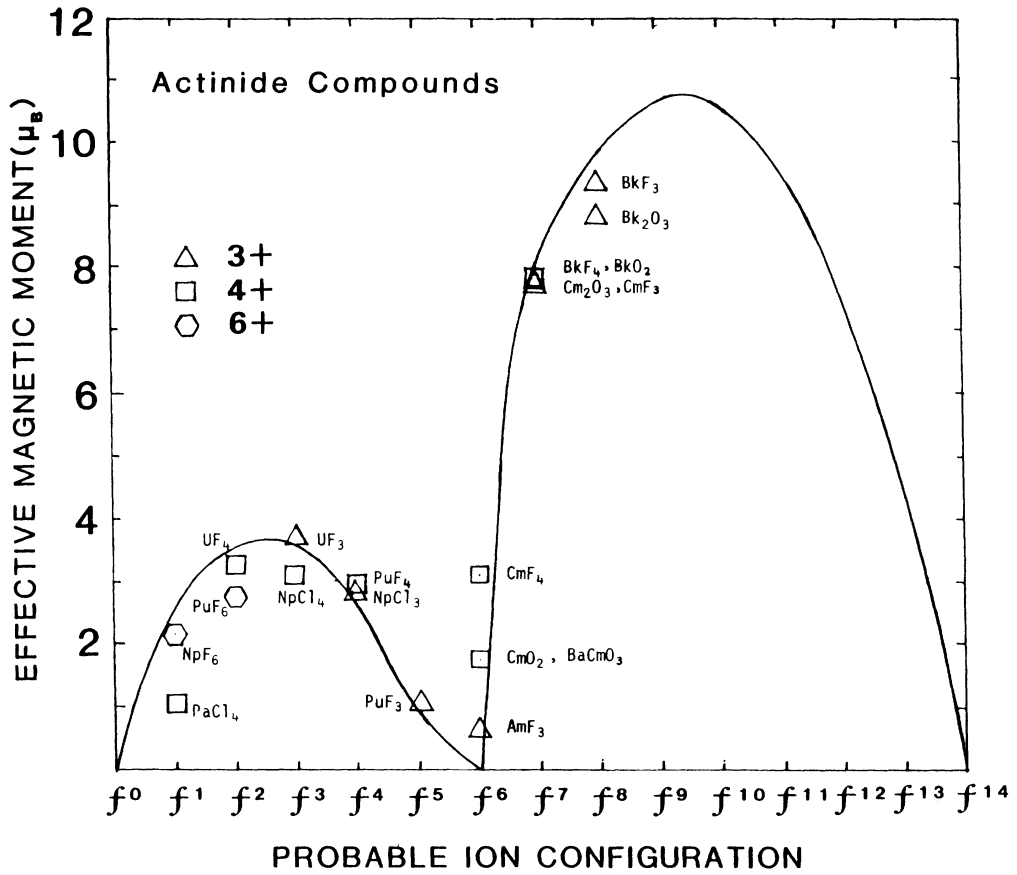

FIG. 9. Experimental effective magnetic moments of actinide compounds as a function of their nominal electronic configuration near 300 K. The solid line connects the theoretical values of expected magnetic moments of the respective ionic configuration using simple *L-S* coupling and Hund's rule for the ground states.

produce the better tetravalent product. Further, the perovskite structure formed by the $BaCmO_3$ compound is known to provide a stabilization for the tetravalent state, as evidenced in part by the greater stability of $BaCmO_3$ vs CmO_2. The stability of the perovskite structure is also seen with the lanthanides; $BaTbO_3$ can be readily prepared in air but TbO_2 is not obtained in air or oxygen atmospheres. Measurements on both the $BaCmO_3$ and CmO_2 samples have given the lowest experimentally measured moment.

If the presence of trivalent curium was to account for the large temperature-dependent susceptibility in the CmF_4 samples, about 14% of the sample mass would need to be in this charge state (assuming susceptibilities are additive and proportional to μ_{eff}^2). This would imply that the CmF_4 samples were actually a mixture of CmF_4 and CmF_3. The curium oxide samples present a different situation. First, the amount of trivalent curium needed to generate the observed nonzero moment would be smaller ($\sim 6\%$) and more difficult to detect. Secondly, the average charge state could occur either as separate phases (Cm_2O_3 with CmO_2) or as a single phase (CmO_{2-x} rather than $CmO_{2.00}$).

In evaluating these results we have considered four possibilities which could account for a nonzero moment in these compounds: (1) The chemical composition of the samples is not stoichiometrically correct, (2) impurities with large moments are present, (3) spin-spin and spin-orbit splittings cause excited states to lie near the ground state and are therefore thermally populated (as found by Van Vleck[3] for europium), and (4) crystal-field splittings are so strong in the compound that the contribution of orbital motion to the magnetic moments are either diminished or quenched. We address these possibilities to varying degrees in the remaining text.

B. X-ray measurements

It is difficult to evaluate stoichiometry and/or purity with the available analytical technique of x-ray diffraction. For example, detection of the 3+ state by x-ray analysis is limited in two ways: (1) Depending on the wavelength of the x-ray beam, only the outer portion of the bulk samples may be analyzed and (2) the detection of a second phase probably requires the presence of 5–10% of that phase.

It is reasonable that the first explanation for nonzero moments in the Cm(IV) compounds would be that a totally tetravalent state had not been achieved, and that some portion of the curium was in the trivalent state. Owing to this possibility, extra attention was given to the preparative methods, and several samples were broken apart to al-

TABLE II. Crystal type and lattice parameters. Error limits on the lattice parameter(s) of an individual sample in this work represent the standard deviation as calculated in the least-squares refinement (8) of the data for that particular sample.

Sample	Crystal type	a_0 (Å)	b_0 (Å)	c_0 (Å)	β (deg.)
CmO_2 no. 1	fcc	5.356(1)			
CmO_2 no. 2	fcc	5.365(1)			
CmO_2 no. 3	fcc	5.364(3)			
CmF_4 (avg)	monoclinic	12.50(2)	10.51(2)	8.16(1)	126.25(10)
AmF_3	trigonal	7.038(4)		7.220(3)	
CmF_3	trigonal	7.012(3)		7.198(5)	
Cm_2O_3	bcc	11.01(1)			
Cm_2O_3	monoclinic	14.22(4)	3.64(1)	8.84(3)	100.5(1)
BkF_4	monoclinic	12.47(5)	10.46(3)	8.13(1)	126.1(1)
BkO_2	fcc	5.332(1)			

low analyses of the central portions. There was no evidence in the x-ray data to support the presence of a second phase (CmF_3 in the CmF_4 samples or lower curium oxides in the CmO_2 samples). The lack of detection of Cm(III) in the CmF_4 by x-ray analyses would suggest that the amount of Cm(III) required to explain the magnetic results was not present in these samples. The situation with the curium oxide samples is less clear. Even though the amount of Cm(III) that would need to be present to explain the magnetic results is smaller, and hence more difficult to rule out, there are two conditions which aid the evaluation of these samples. First, it is easier to detect the presence of a second phase in the diffraction patterns of the fcc CmO_2, or the pseudo—body-centered-cubic (bcc) $BaCmO_3$ samples, as compared to the monoclinic CmF_4 patterns. Secondly, for extensively annealed samples of curium oxide, the presence of a curium oxide other than the pure tetravalent, or trivalent oxide would be expected to be manifested as a single CmO_{2-x} phase rather than having a mixture of two phases (i.e., Cm_2O_3 and CmO_2). In the case of a single substoichiometric CmO_{2-x} phase, as opposed to the presence of two phases, accurately determined lattice parameters should greatly improve the ability to detect any deviation from a pure tetravalent state for curium.

A summary of the x-ray results is given in Table II. The trifluoride preparations all exhibited the trigonal LaF_3-type structure, whereas the tetrafluorides formed the monoclinic, UF_4-type structure. Both monoclinic (Sm_2O_3-type structure) and bcc (Mn_2O_3-type structure) Cm_2O_3 samples were prepared. All lattice parameters are in good agreement with the parameters reported in the literature.[21–24] The $BaCmO_3$ samples were indexed as body-centered-cubic and the parameters were in excellent agreement with data that has been obtained for several $BaAO_3$ compounds ($A = {}_{95}Am$, ${}_{96}Cm$, ${}_{97}Bk$, ${}_{98}Cf$).[25] Our lattice parameters for CmO_2 and BkO_2 both are also in good agreement with published values for these oxides.[26,27]

The value of 5.356(1) Å (derived from 34 diffraction lines) for the lattice parameter of one of the CmO_2 sample is lower than, but in accord with, the average room-temperature value of 5.359(2) Å reported in the literature.[26] Larger lattice parameters would indicate a lower O/Cm stoichiometry and hence a deviation from the tetravalent state. The largest parameter obtained here for a CmO_2 preparation was 5.365 (1) Å. An increase in the lattice parameter of 0.006 Å should be equivalent to 0.02 in the [O]/[Cm] ratio ($CmO_{1.98}$), which reflects an equivalent of 4% Cm(III). Thus, if only single-phase CmO_{2-x} products were obtained in this work, it would appear that in the worst case the stoichiometry of the CmO_2 products did not deviate sufficiently from the tetravalent state to explain the nonzero magnetic moments. But one should note that this is based on the fact that x-ray data in the literature represents material of the correct stoichiometry.

C. Mass spectroscopy measurements and radioassay

Results based on mass spectroscopic and radioassay analyses performed on both the stock solution of ^{248}Cm in HCl and oxide products are shown in Table III. Values given are the maximum observed ppm of impurity to curium by weight. It may be noted that the limited presence of the large-moment lanthanides ${}_{64}Gd$, ${}_{65}Tb$, ${}_{66}Dy$, ${}_{67}Ho$, and ${}_{68}Er$ rules out an explanation of a nonzero average moment based on the presence of a small amount of large-moment impurities. Also, from the purification techniques employed, the most probable lanthanide impurities would be expected to be Pm^{3+}, Sm^{3+}, and/or Eu^{3+}, whose moments range from 0 to $3\mu_B$.

D. Optical-absorption measurements

Optical analyses of the samples in principle should differentiate between Cm(III) and Cm(IV), but this technique also has limitations. Absorption spectra could not be obtained for the opaque CmO_2 and $BaCmO_3$ samples, although excellent spectra were obtained from the CmF_4 and CmF_3 samples. The difficulty in spectral analyses of the latter samples is that the absorptivities of CmF_3 and CmF_4 in solid samples is not known and could not be readily determined with our single-beam spectrophotometer, due in part to the uncertainty of sample path lengths of the solids. Qualitatively, CmF_3 has a simpler spectrum and has a lower absorption than does CmF_4. In the absor-

TABLE III. Impurity analysis (performed by the Analytical Chemistry Division, Oak Ridge National Laboratory). Values given are the maximum observed ppm (weight) of impurity in mass spectroscopic and radioassay analyses on the curium stock solution and the oxide products.

Element	(ppm wt.)	Element	(ppm wt.)
Mass spectroscopy		$_{82}$Pb	2
$_{13}$Al	50	$_{14}$Si	10
$_{5}$B	0.03	$_{50}$Sn	6
$_{56}$Ba	20	$_{73}$Ta	40
$_{20}$Ca	15	$_{22}$Ti	30
$_{24}$Cr	30	$_{74}$W	7
$_{27}$Co	0.3	$_{30}$Zn	5
$_{29}$Cu	2	(masses 147–154)	100
$_{26}$Fe	100	Radioassay	
$_{19}$K	5	$^{155}_{63}$Eu	0.39
$_{57}$La	2	$^{249}_{97}$Bk	0.003
$_{12}$Mg	5	$^{106}_{44}$Ru	0.024
$_{25}$Mn	0.5	$^{137}_{55}$Cs	0.057
$_{11}$Na	2	Sum of all other radionuclides	0.001
$_{28}$Ni	50		sum = 483 ppm
$_{15}$P	0.3		

bance spectra of the CmF_4 samples, an absorbance due to Cm(III) could not be detected [a major Cm(III) absorption occurs at ~ 600 nm where there is a minimum in the Cm(IV) absorption], supporting the contention that the samples contained much less than the 14% Cm(III) needed to explain the magnetic results.

The spectral wavelengths and intensities for the spectrum of the CmF_4 sample (Fig. 10) are consistent with the solid Cm^{4+} spectrum of Asprey,[28] and includes the third through the fourteenth lowest excited states. The lower solid lines indicate the experimental absorption wavelengths and intensities obtained by Asprey[28] for CmF_4, while the upper solid lines indicate the theoretical wavelengths predicted by Conway[29] by choosing splitting parameters for Cm^{4+} ions via a least-squares fit. This treatment predicts a relatively high first excited state, $J=1$, at 0.41 eV above the $J=0$ ground state for CmF_4, and suggests a negligible population of this state for temperatures below 300 K. Absorption spectra for our CmF_3 samples are in agreement with spectra for aqueous Cm^{3+} ions,[28] and indicate a very high first excited state, $J=\frac{7}{2}$, at $\Delta=2.10$ eV above the ground state.

The absorption bands for the AmF_3 sample (Fig. 11) are consistent with values reported by Hessler[4] for Am^{3+} ions in solution, and represent transitions from the fourth

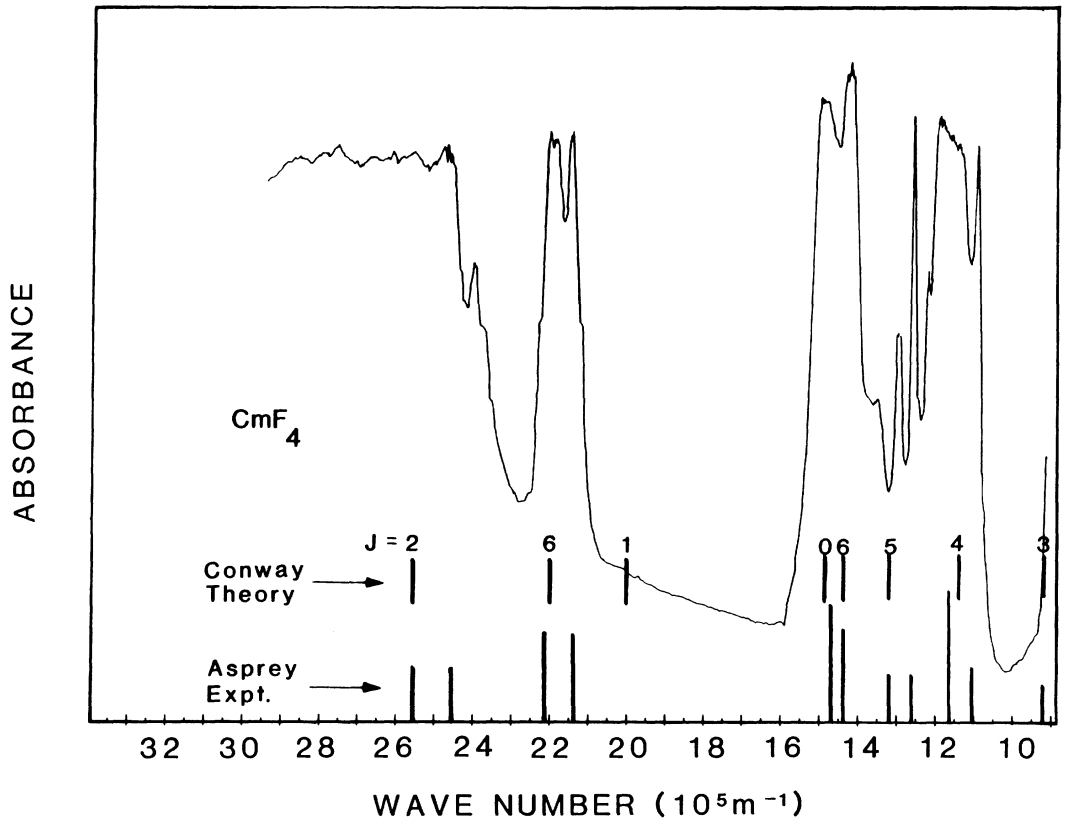

FIG. 10. Optical transmission of a CmF_4 sample as a function of the reciprocal wavelength of photons. The bottom set of lines correspond to the reciprocal wavelengths and intensities of experimental absorption lines for Cm^{4+} in solution according to Asprey (Ref. 28). The top set of lines correspond to the theoretical energies of the excited states of a $5f^6$ configuration according to Conway (Ref. 29).

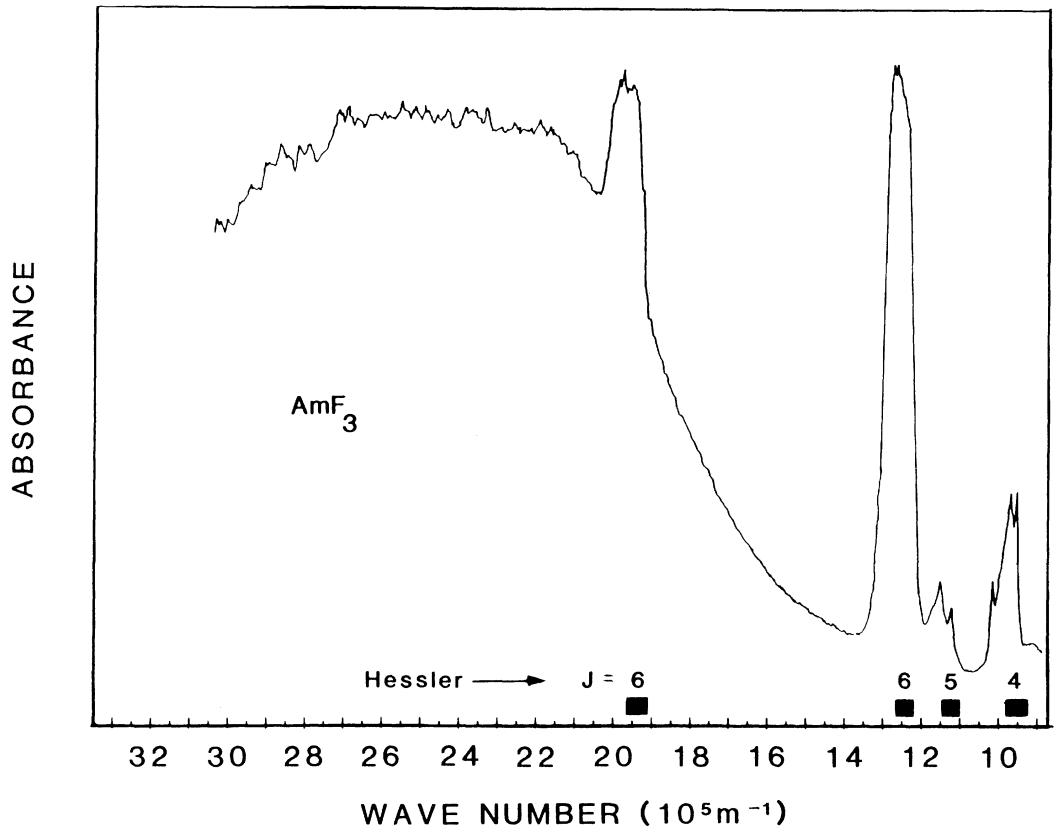

FIG. 11. Optical transmission of an AmF_3 sample as a function of the reciprocal wavelength of photons having energies between 1 and 3 eV. The solid bars indicate the reciprocal wavelengths of strong absorption bands for aqueous Am^{3+} ions and the value of J indicates the total-angular-momentum quantum number of the excited state to which the $^7F_0$ ground state makes its transition.

through the seventh lowest excited states. The solid bars along the abscissa indicate the absorption wavelengths for the Am^{3+} aqueous ions above 9×10^3 cm^{-1}. Spectral parameters derived from a theoretical fit to even higher excited states[29] place the first excited state, $J=1$, at $\Delta=0.33$ eV (2.7×10^3 cm^{-1}) above the $J=0$ ground state for the solution. Unless crystal fields substantially split the $J=1$ state for the AmF_3 in the low absorbance region, this state is too high to allow significant thermal population at 300 K ($e^{-\Delta/kT}\sim10^{-5}$).

The fact that the higher substates of both AmF_3 and CmF_4 show hyperfine splitting in the optical spectra (see Figs. 10 and 11), would lead one to conclude that a crystal field exists at the actinide atom. However, in all of these arguments it has been assumed that the f^6 ground state ($J=0$) will have a zero moment since it has only the $M_J=0$ substate and should not be further split by even a substantial crystal field at the actinide atom. The remaining unlikely explanation for the observed nonzero moments is that crystal-field splittings are so large that the $J=1$ first excited state has a very low-lying substate. The small magnitude of the hyperfine splitting observed for the higher energy levels makes it unlikely that such a large splitting exists for the first excited state. In addition, the agreement of the magnetic results for the two crystal forms of Cm_2O_3 tends to rule out such large crystal-field effects. Therefore, as far as thermal effects are concerned, we would expect negligible population of excited states in these samples for temperatures up to 300 K.

IV. CONCLUSIONS

Results from magnetic measurements of several compounds which nominally exhibit the $5f^6$ electronic structure are not consistent with a zero moment, as predicted by the classic theory based on Hund's-rule and either L-S or intermediate coupling. Neither sample stoichiometry nor the presence of large-moment impurities offer a satisfactory explanation for these nonzero moments. Attempts to explain these differences as arising from low-lying excited states or from crystal-field splittings were likewise unsatisfactory. This leads one to consider if simple free-ion theory is adequate for these particular actinide compounds although it provides a value for the magnetic moment which is in reasonable agreement with the experimentally measured values for most of the other actinide compounds in Fig. 9. It should be emphasized that magnetic measurements provide a sensitive indicator of perturbations on the $5f^6$ electronic configuration (bonding, hybridization, etc.) as evidenced by the large change in magnetic moment [(0—8)μ_B] brought about by the addition of a single electron. It is in fact surprising that the actinide compounds with a $5f^7$ configuration gave good agreement

with the classic predictions, since the magnetic ordering and large Θ values for Cm_2O_3 and BkO_2 indicate these $5f^7$ ions are not isolated. Thus, from our results we conclude that additional studies on the $5f^6$ and $5f^7$ configurations are necessary, and that the factors discussed here must be carefully considered in future experimental and theoretical work.

ACKNOWLEDGMENT

This research was sponsored by the Division of Chemical Sciences, Office of Basic Energy Sciences, U.S. Department of Energy, under Contracts Nos. DE-AS05-79ER10348 with the University of Tennessee (Knoxville) and W-7405-eng-26 with Union Carbide Corporation.

[1]Charles Kittel, in *Introduction to Solid State Physics,* 3rd ed. (Wiley, New York, 1967), p. 482.

[2]J. H. Van Vleck, in *The Theory of Electric and Magnetic Susceptibilities* (Oxford University Press, London, 1932), p. 244.

[3]J. H. Van Vleck, in *The Theory of Electric and Magnetic Susceptibilities* (Oxford University Press, London, 1932), p. 245.

[4]J. P. Hessler and W. T. Carnall, ACS Symp. Ser. 131, 349 (1980).

[5]S.-K. Chan and D. J. Lam, in *The Actinides: Electronic Structure and Related Properties,* edited by A. J. Freeman and J. B. Darby, Jr. (Academic, New York, 1974), Vol. I, pp. 15–21.

[6]W. T. Carnall and B. G. Wybourne, J. Chem. Phys. 40, 3428 (1964).

[7]R. D. Baybarz, J. B. Knauer, and P. B. Orr, U.S. Atomic Energy Commission Document No. ORNL-4672 (unpublished).

[8]L. J. King, J. E. Bigelow, and E. D. Collins, ACS Symp. Ser. 161, 41 (1981), and references therein.

[9]T. D. Chikalla and L. Eyring, J. Inorg. Nucl. Chem. 31, 85 (1969).

[10]D. K. Williams, U.S. Atomic Energy Commission Document No. IS-1052 (unpublished).

[11]Analytical Chemistry Division, Oak Ridge National Laboratory.

[12]J. P. Young, R. G. Haire, R. L. Fellows, and J. R. Peterson, J. Radioanal. Chem. 43, 479 (1978).

[13]S. E. Nave and Paul G. Huray, Rev. Sci. Instrum. 51, 5 (1980).

[14]S. A. Marei and B. B. Cunningham, J. Inorg. Nucl. Chem. 34, 1203 (1972).

[15]L. R. Morss, J. Fuger, J. Goffart, and R. G. Haire, J. Inorg. Chem. 22, (1982).

[16]E. A. Boudreaux and L. N. Malaxc, in *Theory and Applications of Molecular Paramagnetism* (Wiley, New York, 1976), p. 303, and references therein.

[17]J. Samuel Smart, *Effective Field Theories of Magnetism* (Saunders, Philadelphia, 1966), p. 58.

[18]Basil Kanellakopulos, Clemens Aderhold, and Ernst Domberger, Radiochim. Acta 25, 89 (1978).

[19]D. J. Lam and A. T. Aldred, in *The Actinides: Electronic Structure and Related Properties,* edited by A. J. Freeman and J. B. Darby, Jr. (Academic, New York, 1974), Vol. I, p. 109 (a review with references to most of the earlier work.)

[20]S. E. Nave, R. G. Haire, and P. G. Huray, University of California at Berkeley Report No. LBL-12441 (unpublished).

[21]L. B. Asprey and T. K. Keenan, Inorg. Chem. 4, 985 (1965).

[22]L. B. Asprey and R. G. Haire, Inorg. Nucl. Chem. Lett. 9, 1121 (1973) and references therein.

[23]H. O. Haug and R. D. Baybarz, Inorg. Nucl. Chem. Lett. 11, 847 (1975).

[24]W. C. Mosley, J. Am. Ceram. Soc. 54, 475 (1971).

[25]J. Bourges and R. G. Haire (unpublished).

[26]J. R. Peterson and J. Fuger, J. Inorg. Nucl. Chem. 33, 4111 (1971).

[27]J. Fahey, R. P. Turcotte, and T. D. Chikalla, J. Inorg. Nucl. Chem. 10, 459 (1974).

[28]L. B. Asprey and T. K. Keenan, J. Inorg. Nucl. Chem. 7, 27 (1958).

[29]J. G. Conway, J. Chem. Phys. 40, 904 (1964).